## PAPER

# Removal of typical pollutant ciprofloxacin using iron–nitrogen co-doped modified corncob in the presence of hydrogen peroxide†

Yuankun Liu, [ID] * Xinxia Zhang and Hongrun Liu

Iron–nitrogen co-doped modified corncob (Fe–N-BC) was synthesized using a hydrothermal and calcination method. The material shows excellent oxidation performance and environmental friendliness. When the dosage of Fe–N-BC was 0.6 g L$^{-1}$, the concentration of H$_2$O$_2$ was 12 mM and pH was 4, ciprofloxacin (CIP) was virtually totally eliminated in 240 min under Fe–N-BC/H$_2$O$_2$ conditions. The TOC removal efficiency was 54.6%, and the effects of various reaction parameters on the catalytic activity of Fe–N-BC were thoroughly assessed. Through electron paramagnetic resonance (EPR) analyses and free radical quenching experiments, it was established that the reactive oxygen species ($^{\bullet}$OH, $^{\bullet}$O$_2^-$, $^1$O$_2$) were crucial in the elimination of CIP. Furthermore, the degradation of CIP was accelerated by the synergistic interaction between the transition metal and PFRs. A thorough evaluation was conducted to assess the respective contributions of adsorption and catalytic oxidation in the system. The degradation mechanism of CIP was proposed under Fe–N-BC/H$_2$O$_2$ conditions. Meanwhile, the possible degradation intermediates and pathways were proposed, and the toxicity of the degradation products of CIP was also meticulously investigated in the study. These findings offered the elimination of CIP in water a theoretical foundation and technical support.

## 1. Introduction

The development of the medical industry has led to an increase in pharmaceutical wastewater discharge. Pharmaceutical wastewater has become one of the most difficult and dangerous types of wastewater to treat because of its high toxicity and complexity in degradation.[1–3] In particular, antibiotics are among the most commonly used in medicine, which cause a serious threat to the water environment.[4,5] Ciprofloxacin (CIP) is a widely used fluoroquinolone antibiotic that is frequently found as the decomposition product of another widely used antibiotic, enrofloxacin.[6–8] Ciprofloxacin, a fluoroquinolone of the second generation, has a stable molecular structure and is resistant to biotransformation and degradation in water.[9,10] In aquatic environments, the residual ciprofloxacin concentration varies from ng L$^{-1}$ to mg L$^{-1}$, with a high of 31 mg L$^{-1}$.[11,12] Extreme pollution and ecological risk are caused by ciprofloxacin residues, such as the suppression of normal microorganism activity and the spread of antibiotic resistance.[13,14]

However, utilizing conventional wastewater treatment techniques, such as physical, chemical and biological treatment, it is difficult to handle the issue of antibiotic residues.[15,16] As a result, developing effective technology for removing ciprofloxacin from the environment is both required and urgent.

The advanced oxidation process (AOP), which is viewed as a possible substitute to conventional treatment methods because of its efficiency and low environmental impact, can be used to remove antibiotics from water.[2,17] They have the ability to produce reactive oxygen species (ROS) in the environment with little selectivity and high reactivity, including hydroxyl, superoxide and sulfate radicals.[18] Most organic molecules can react with ROS fast, resulting in their full mineralization into less hazardous smaller components, even CO$_2$ and H$_2$O.[19] The Fenton reaction based on the hydroxyl radical has become one of the most studied and employed AOPs because of its rapid reaction time, high efficiency, easy operation, and lack of toxicity.[20] However, the pH range of conventional homogeneous Fenton is limited and produces a large amount of iron sludge.[21] In order to solve the above problems, it is necessary to improve the Fenton reaction efficiency by optimizing the operating conditions and developing new Fenton/Fenton-like catalysts.

Carbon-based materials (such as activated carbon (AC), graphene oxide (GO), carbon nanotubes (CNTs), *etc.*) have attracted more and more attention in the Fenton (or Fenton-like) system used in the degradation of organic pollutants.[20,22]

*Municipal Engineering Department, College of Civil Engineering and Architecture, Beijing University of Technology, Beijing 100124, P. R. China. E-mail: liuyuankun@bjut.edu.cn; zhangxinxia1999@163.com; liuhr@emails.bjut.edu.cn; Fax: +86-10-6739-1726; Tel: +86-10-6739-1726*

† Electronic supplementary information (ESI) available. See DOI: https://doi.org/10.1039/d3ra06437a

However, most of the carbon-based materials are expensive. Biochars (BCs) prepared from agricultural and industrial wastes are relatively inexpensive and environmentally friendly, which are used as an adsorption material for the removal of organic pollutants.[23,24] Corncob is particularly strong in water absorption and adsorption properties due to its relatively homogeneous organization and internal reticulation. At the same time, corncob is an abundant biodegradable material with high strength, high stiffness and low weight. Due to the structural characteristics of BCs, it can promote $Fe(II)/Fe(III)$ redox cycling through various mechanisms. (1) With electron-rich oxygen-containing functional groups and abundant persistent free radicals (PFRs), BCs can act as electron donors to directly provide electrons to facilitate $Fe(III)$ reduction.[25] (2) The chemical bond formed between the BCs and the iron-containing material can lower the redox potential of $Fe(III)$, which is favorable for the reduction of $Fe(III)$.[26] In addition, the application of pristine biochar in advanced oxidation systems is limited because of poor types of functional groups.[27] In recent years, various modification methods were used to modify materials. It showed that nitrogen-doping can effectively improve the function of electrical conductivity of the carbon matrix and the activity of catalyst can also be improved. However, this nitrogen-doped biochar was difficult to recycle.[28] Iron is widely used for its excellent magnetic and redox properties.[29] Therefore, the iron–nitrogen co-doped modified biochar synthesized can enhance catalyst activity and the material can separate easily from the solution at the same time.

In this work, modified biochar with iron–nitrogen co-doping (Fe–N-BC) was synthesized by pyrolysis of corncob, urea and iron salt. The impacts of various preparation conditions on the adsorption of ciprofloxacin were studied. The best preparation scheme was selected, and its physical and chemical properties were analyzed. The effect of the removal ciprofloxacin was studied in Fe–N-BC/$H_2O_2$ system under different conditions, including hydrogen peroxide concentrations, catalyst dosages, pH, and initial CIP concentrations. The degradation mechanism of CIP was analyzed by quenching test and electron paramagnetic resonance (EPR) in Fe–N-BC/$H_2O_2$ condition. After systematically evaluated the role of catalytic oxidation and adsorption in the system, the degradation pathway of CIP was proposed in the study.

## 2. Materials and methods

### 2.1. Chemicals

Corncob powders (100 meshes) were obtained from agricultural products processing of Shandong in China. Ciprofloxacin (CIP, $C_{17}H_{18}FN_3O_3$, 98%) was bought from Energy Chemical. Ferrous sulfate heptahydrate ($FeSO_4 \cdot 7H_2O$, ≥99.0%), urea ($CH_4N_2O$, 99.0%), ascorbic acid ($C_6H_8O_6$), tertbutyl alcohol (TBA), $p$-benzoquinone ($p$-BQ), potassium iodide (KI), and furfuryl alcohol (FFA) were purchased from Aladdin Biochemical Corporation. Hydrochloric acid (HCl) and sodium hydroxide (NaOH) were bought from Sinopharm. All of the chemicals were analytically pure, and all solutions were configured with ultrapure water.

### 2.2. Synthesis of catalysts

Before use, different batches of corncob powder were mixed thoroughly then were washed and dried naturally. Iron–nitrogen co-doped modified biochar (marked as Fe–N-BC) was synthesized by hydrothermal and calcination method. Firstly, 50 mL of ultrapure water was used to dissolve 5.56 g of $FeSO_4 \cdot 7H_2O$, 2.5 g of ascorbic acid (a reducing agent), and urea (a source of nitrogen). Secondly, 3 g corncob was added into the mixed solution and the mixture was then heated at 160 °C for 10 h in a high-pressure reactor. And it was dried at 80 °C for 24 h. Finally, it was put into the quartz boat and heated to 800 °C (10 °C min$^{-1}$) for 1 h. The cooled product was ground and sifted (100 meshes). At the same time, the material in the absence of urea (marked as Fe-BC), and the material with only corncob powders (marked as BC) were also prepared in the similar way, respectively.

### 2.3. Characterization

Scanning electronic microscope (SEM, SU8020, Japan) was used to investigate the characteristics and morphology of catalysts. The specific surface areas ($S_{BET}$) and average pore diameters of catalysts were measured by the Brunauer–Emmett–Teller (BET, Micromeritics ASAP 2460, USA). The composition phases of catalysts were identified by X-ray diffraction (XRD, BRUCKER D8 Advance, Germany) in $2\theta$ from 5° to 90°. Additionally, Fourier transform infrared spectroscopy (FTIR, Nicolet 6700) within the wavenumber range of 4000–400 cm$^{-1}$ was used to determine the structural information of catalysts. The BKT-4500 vibration sample magnetometer was used to conduct VSM analysis of fresh and used Fe–N-BC.

### 2.4. Experimental section

The experiments of catalytic degradation, influence factor and catalyst reuse were conducted at 25 °C and 250 rpm on the shaking table. The pH of the CIP solution was adjusted before to the process using either 1 M HCl or 0.1 M NaOH. And the removal reaction of CIP was performed to start the reaction by adding the catalyst and $H_2O_2$ into 100 mL CIP solution. At predetermined intervals, a specific amount of solution was extracted using plastic syringes, and the samples were then filtered through a 0.45 μm membrane for detection. All above the experiments were repeated twice.

### 2.5. Analytic methods

The absorbance of the solution was measured using a UV-vis spectrophotometer (UV-1900, Shimadzu, Japan) at 277 nm. A Multi TOC/TN Analyzer (vario TOC, Germany) was used to measure the total organic carbon (TOC) content. Electron paramagnetic resonance (EPR, BRUCKER A300-10/12, Germany) was used to quantify the contribution of reactive oxygen species (ROS) in the reaction system. The products of CIP degradation were identified by HPLC-MS (Agilent 1290 Infinity/6460 LC/QQQ MS). The mobile phase was performed at a flow rate of 0.4 mL min$^{-1}$ with acetonitrile aqueous solution as eluent A and 0.1% formic acid solution as eluent B (20/80 v/v)

and a 20 μL volume of the sample was injected. According to previous study, the mass spectral analysis was conducted in positive mode over a mass range of 100–400 *m/z* and the capillary temperature was 300 °C.[30]

# 3. Results and discussion

## 3.1. Characterization of the catalysts

As shown in Fig. 1(a), the surface characteristics and microstructure of BC and Fe–N-BC materials were determined by SEM. The surface morphology of BC was irregular, fluffy and porous. It was caused by the pyrolysis process.[31] As shown in Fig. 1(b), the surface of Fe–N-BC material contains a significant number of crystal particles. These particles may mainly be ferric oxide crystals.[28] Compared with the BC, the metal iron was successfully loaded.

Using the $N_2$ adsorption–desorption isotherm, the surface area and pore structure of the two materials before and after modification were determined. The $S_{BET}$ of BC and Fe–N-BC were 132.512 and 261.772 $m^2$ $g^{-1}$, respectively, and the detailed data were shown in Table S1.† Both materials exhibit typical type IV isotherms with obvious adsorption hysteresis loops in Fig. 1(c), which is due to the capillary coalescence system generated by the porous adsorbent materials.[32] The
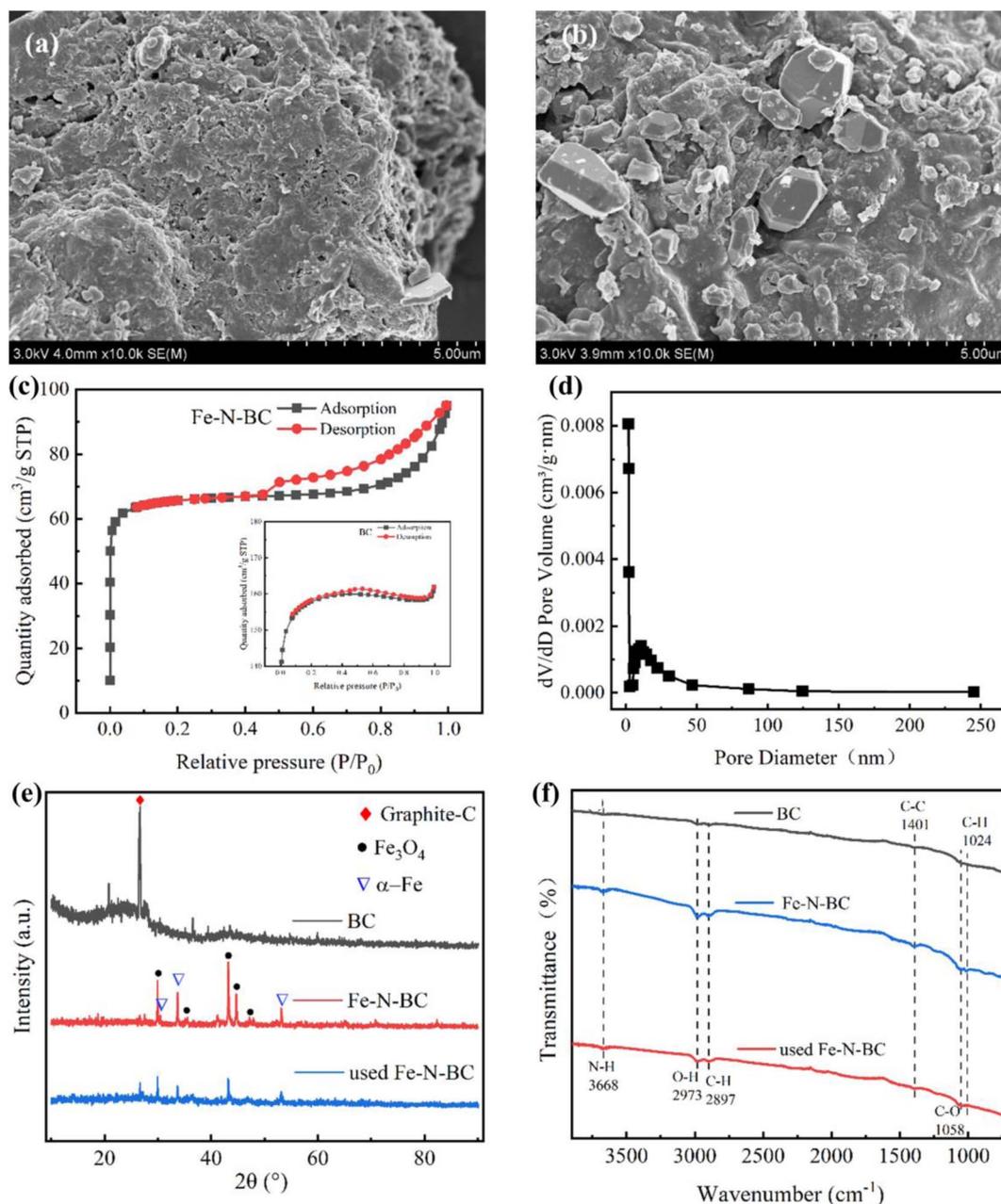


Fig. 1 SEM images of (a) BC and (b) Fe−N-BC; (c) $N_2$ adsorption–desorption isotherms of Fe−N-BC and BC (inset); (d) pore size distribution of Fe−N-BC; (e) XRD pattern and (f) FTIR spectra.

formation of a fluffy structure in the presence of urea is the cause of the comparatively greater BET surface area of Fe–N-BC compared to BC.[33] The higher specific surface area gives the composite a better adsorption capacity and an abundance of active sites for activating $H_2O_2$.

The material composition and phase of the sample were determined using XRD analysis. In Fig. 1(e), the diffraction peak of BC occurred at about 26°, corresponding to the (002) graphitized carbon.[34] The diffraction peaks of Fe–N-BC at $2\theta$ values of 30.4°, 35.5°, 43.2°, 44.6°, and 47.1° correspond to the (002), (111), (102), (110), and (331) crystal types of $Fe_3O_4$.[35] Furthermore, the diffraction peaks at 30.4°, 33.7°, and 53.1° were caused by $\alpha$-Fe. The peak location of the used Fe–N-BC did not differ considerably from Fe–N-BC. It demonstrated that the crystal structure of the catalyst was stable and the peak abundance somewhat altered after the reaction, indicating that iron was involved in the catalytic process.

As shown in Fig. 1(f), compared with BC, the peak intensity of Fe–N-BC at 3668 $cm^{-1}$ decreased significantly, due to the vibration of the N–H bond stretching. It indicated that N was successfully doped on Fe–N-BC.[36] The stretching vibration band at 2973 $cm^{-1}$ was associated with the hydroxyl (–OH) in the carboxyl and phenolic groups of Fe–N-BC.[37] Compared to previously used Fe–N-BC, the peak strength of Fe–N-BC was greater. It demonstrated that a significant amount of carboxyl and hydroxyl groups took part in the catalytic activity, which led to the consumption of oxygen-containing groups with functional properties. The peaks at 2897 and 1401 $cm^{-1}$ were generated by the vibration of the C–H bond and the skeletal vibration of the C–C single bond, respectively.[38,39] Consequently, Fe–N-BC exhibited a significant abundance of oxygen-containing functional groups and the oxygen-containing functional groups were reduced after the reaction. It can be inferred that the oxygen-containing groups with functions of Fe–N-BC material involve in the catalytic oxidation process.

Fe–N-BC showed a typical S-type hysteresis loop and the residual magnetic value and coercivity value of the materials were almost similar in Fig. 2. The saturation magnetization of fresh and used Fe–N-BC was 12 and 9 emu $g^{-1}$, respectively. After the reaction, the saturation magnetization of Fe–N-BC decreased slightly. It may be due to the dissolution of iron ions during the catalytic reaction in the catalyst. However, the net magnetism of the utilized Fe–N-BC was still sufficient to successfully separate it from the mixture. It demonstrated that Fe–N-BC had excellent magnetic capabilities.

## 3.2. Heterogeneous Fenton catalytic activities

**3.2.1. Optimization of Fe–N-BC/$H_2O_2$ process for CIP degradation.** The mass ratio of corncob to urea with the best CIP degradation performance was searched by setting the ratios as 1 : 0, 1 : 1, 1 : 2 and 1 : 3, respectively. As shown in Fig. 3, when the urea doping amount increased from 0 to 1, the adsorption efficiency of ciprofloxacin increased slightly. When the mass ratio of biomass to urea was 1 : 1, the adsorption efficiency was 39.33%. It may be due to the slight increase of adsorption sites due to nitrogen doping. Then the adsorption efficiency decreased with the increase of doping amount. It may be due to the adsorption sites were occupied by excess urea. In addition, under the condition of Fe–N-BC/$H_2O_2$, the degradation efficiency of ciprofloxacin was the highest (98.25%) when the radio was 1 : 1. The reason was that nitrogen doping was thought to be a useful technique for modifying spin density and charge distribution to enhance the catalytic performance of carbonaceous materials.[40] Nitrogen doping provided more catalytic oxidation and adsorption active sites for the removal of ciprofloxacin.[41] Thus, it can improve the performance of the catalyst. Therefore, for subsequent experiments in this study, a catalyst with a mass ratio of biomass to urea of 1 : 1 was chosen.

In Fig. 4(a), under the presence of $H_2O_2$ alone, only 12.45% CIP can be removed. It showed that $H_2O_2$ was difficult to oxidize CIP without catalyst activation. The large specific surface area of the material is favorable for the adsorption of CIP, and the experimental results showed that the adsorption rates of Fe-BC and Fe–N-BC on CIP were 36.69% and 39.95%, respectively. Meanwhile, the FPRs generated during the BC pyrolysis process could also be used to degrade CIP, so that some CIP could still be removed in the absence of $H_2O_2$ in the system. Previous studies have shown that BC can activate oxidants.[42] Compared with the adsorption of CIP by BC, the removal effectiveness of CIP in BC/$H_2O_2$ condition was slightly increased by 7.02%. The
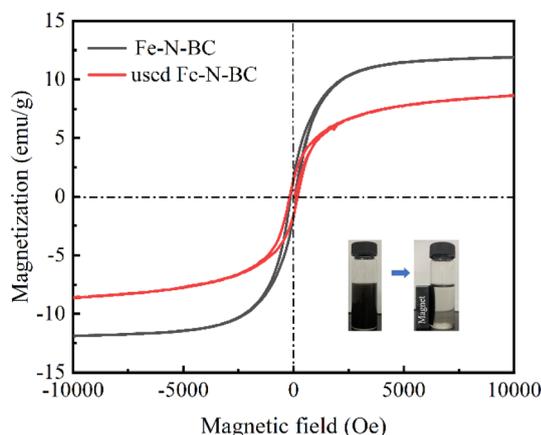


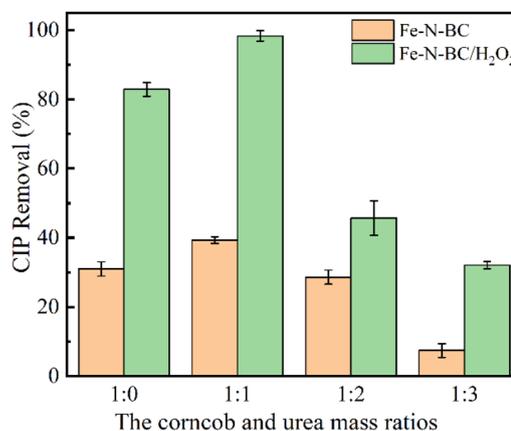Fig. 2  Magnetization curves of fresh and used Fe–N-BC.



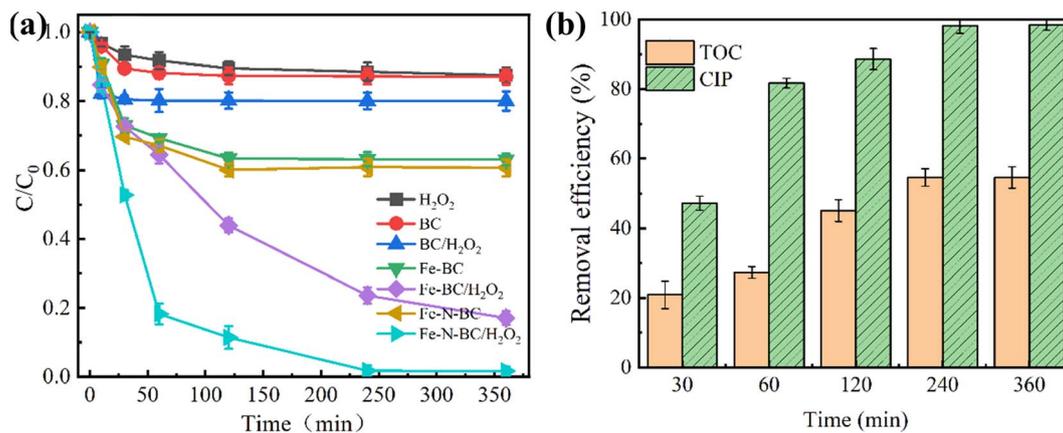Fig. 3  Removal of CIP at different corncob and urea mass ratios.

Fig. 4 (a) The removal efficiency of CIP in various systems. (b) TOC removal efficiency in the Fe−N-BC/$H_2O_2$.

removal efficiency of ciprofloxacin was 98.25% in 240 minutes and the removal efficiency of TOC was 54.6% when the concentrations of $H_2O_2$ were 12 mM and the dose of Fe−N-BC was 0.6 g $L^{-1}$. The description of the entire reaction process is shown in Text S1.† In addition, almost all removal of CIP and high mineralization efficiency were due to adsorption and Fenton-like reactions. $Fe^0$ and $Fe_3O_4$ were present in the catalyst caused by the activation of hydrogen peroxide. The excellent catalytic performance of Fe−N-BC in comparison to other materials suggested that Fe might be the primary active component. Compared with Fe-BC/$H_2O_2$ condition, the removal efficiency increased by 15.42% in Fe−N-BC condition. It demonstrated that nitrogen doping can substantially increase the capacity of $H_2O_2$ to activate. The explanation was that it
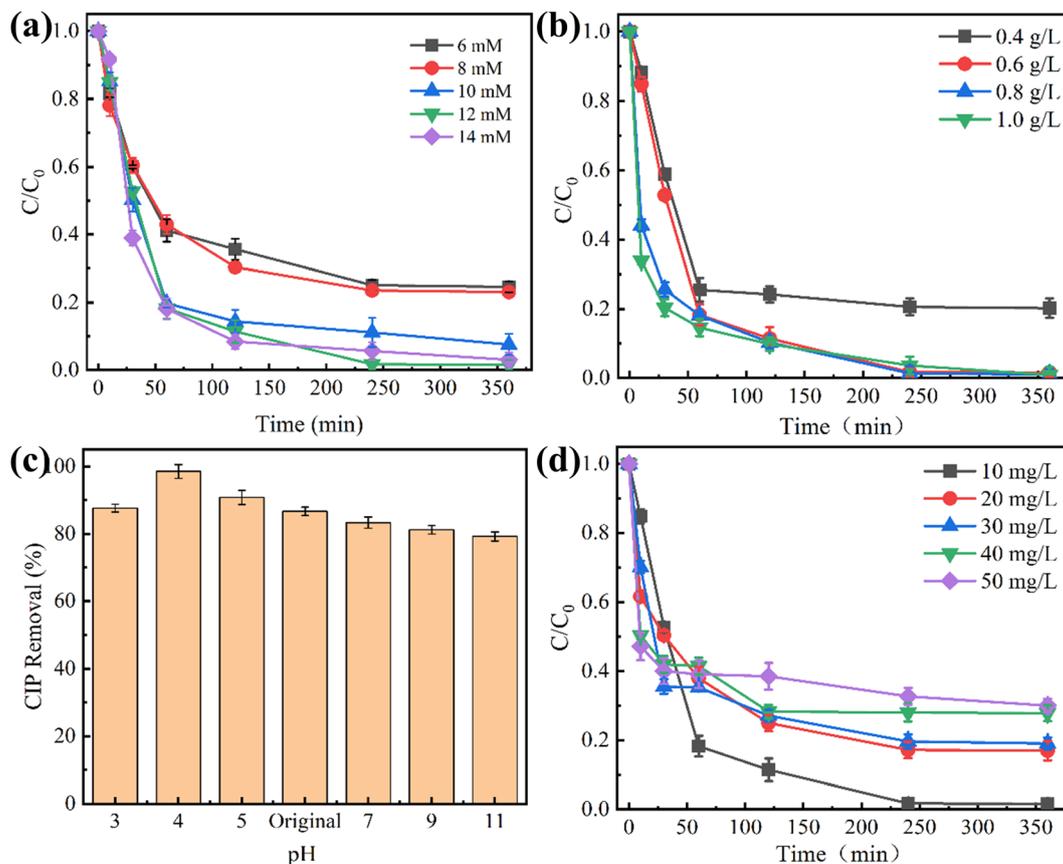


Fig. 5 The impact of various factors on the CIP degradation in Fe−N-BC/$H_2O_2$: (a) effect of $H_2O_2$ concentration, (b) effect of catalyst dosage, (c) effect of initial pH value and (d) effect of initial CIP concentration. Reaction conditions: initial CIP, 10 mg L; pH, 4; $H_2O_2$, 12 mM; catalyst dosage, 0.6 g $L^{-1}$.

might boost the carbon matrix's conductivity and offer additional active sites for catalysis.[43] In addition to adjusting the electrical structure of carbon catalysts, iron and nitrogen doping modified corncob may also decrease metal leaching.[29] According to characterize VSM, Fe–N-BC has good magnetic and easy recycling.

**3.2.2. Factors influencing the efficiency of the Fe–N-BC/H₂O₂ system.** The removal efficiency of CIP significantly improved from 74.89% to 98.25% when the concentration of hydrogen peroxide increased from 6 mM to 12 mM (Fig. 5(a)). The reason was that can activate hydrogen peroxide to generate more $^•$OH, which was a major factor in the decomposition of CIP.[44] Nevertheless, when excessive addition of hydrogen peroxide to 14 mM led to self-scavenging of a small amount of $^•$OH, the removal efficiency of CIP hardly decreased. This was due to the presence of other reactive oxygen species (ROS) with substantial oxidation capacities in addition to hydroxyl radicals.

As shown in Fig. 5(b), the impact of Fe–N-BC dose on the removal of CIP was studied. The removal efficiency of CIP within 240 min was 79.4% and 98.25% when the dose of Fe–N-BC was 0.4 g L$^{-1}$ and 0.6 g L$^{-1}$, respectively. These findings demonstrated that boosting the dosage of Fe–N-BC can increase the amounts of active sites available for activating H₂O₂ and producing $^•$OH. However, while the catalyst dosage was increased further to 0.8 and 1.0 g L$^{-1}$, the final removal efficiency of CIP was almost unchanged. Hydroxyl radicals may self-clear as a result of adverse reactions. In subsequent tests, to reduce the amount of catalyst and save costs, 0.6 g L$^{-1}$ was choosen as the optimal dose of catalyst.

One of the most crucial factors in advanced oxidation reactions was the initial pH. It had an impact on the stability of the catalyst in Fe–N-BC, the activity of the oxidant, and the release of ferrous ions. Therefore, it was necessary to investigate the effect of various initial pH of solution on CIP removal. CIP was almost completely removed in 240 min when the initial pH was 4 in Fig. 5(c). The removal rate decreased slightly to 87.57% and 90.82%, when the initial pH value was 3 and 5, respectively. However, the removal efficiency of ciprofloxacin was still 79.19% when the pH was adjusted to 11. According to these findings, Fe–N-BC/H₂O₂ shown outstanding catalytic performance for the elimination of CIP throughout a wide pH range (3.0–11.0). It was sufficient for wastewater treatment.

According to the data presented in Fig. 5(d), it can be observed that the removal effectiveness of ciprofloxacin (CIP) exceeded 70% after a reaction time of 240 min when the initial concentration of ciprofloxacin ranged from 10 to 50 mg L$^{-1}$. The elimination effectiveness of CIP steadily declined as the concentration of original pollutants increased. Therefore, the reasons were speculated as follows: with the increase of CIP concentrations, the adsorption site of Fe–N-BC was fixed, resulting in the decrease of CIP adsorption efficiency.[29] In addition, the ratio of CIP to catalyst increased gradually, and the removal capacity of contaminants per unit mass of catalyst was limited. This contributed to a decrease in the ratio of active substances to CIP and a gradual decrease in CIP removal.[45] The degradation process was accompanied by the formation of a large number of intermediates. These intermediates also
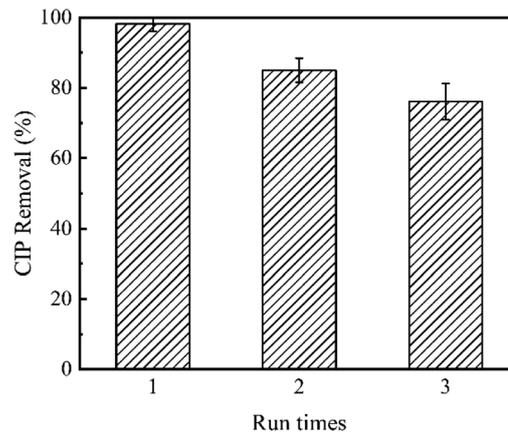


Fig. 6 The removal efficiency of three repeated reactions.

consume the reactive oxygen species, which will compete with CIP and eventually reduce the degradation efficiency of CIP.[46]

**3.2.3. Reusability and stability of Fe–N-BC.** In practical application, the reusability of catalysts is a crucial factor. Consequently, the repeatability of Fe–N-BC was examined in this study. In Fig. 6, the removal effectiveness of CIP gradually declined as the number of cycles increased. Notably, the degradation efficiency of CIP was still about 76.09% after three cycles, and the leaching amount of iron ions was almost zero. Therefore, the biochar group in Fe–N-BC had a strong protective effect on iron leaching, and the catalyst had high reusability and stability for the degradation of organic pollutants. Furthermore, no metal ions were leached from the Fe–N-BC catalyst during the catalytic reaction process, unlike in earlier investigations.[41] It has a low pollution to the environment. So, it had a broad application prospect as a catalyst to improve the organic pollutants in aqueous solution.

### 3.3. The degradation mechanisms

**3.3.1. Analysis of active species.** In order to confirm the existence of different reactive oxygen species (ROS) in Fe–N-BC/H₂O₂ condition, DMPO and TEMP were used as free radical spin trapping agents to conduct EPR tests, respectively. DMPO was first used to detect hydroxyl radical ($^•$OH). The characteristic peak (1 : 2 : 2 : 1) of the DMPO-$^•$OH adduct's usual EPR signal can be seen in Fig. 7(a). It indicated that $^•$OH can be generated in Fe–N-BC/H₂O₂ condition. Additionally, the signal strength of the DMPO-$^•$OH adduct was dramatically increased for 10 min as compared to the EPR signal of 1 min. Superoxide radical ($^•$O₂$^-$) was also captured by DMPO, and EPR signal of quadruple characteristic peak was monitored and attributed to DMPO-$^•$O₂$^-$ signal (Fig. 7(b)). In addition, singlet oxygen ($^1$O₂) was captured by TEMP to generate a representative triple characteristic peak (1 : 1 : 1). As shown in Fig. 7(c), $^1$O₂ was generated in Fe–N-BC/H₂O₂ condition by comparing the signal intensity at 1 min and 10 min. These findings demonstrated that under the Fe–N-BC/H₂O₂ conditions, both free radicals and non-free radicals participated in the degrading process.

Further studies were conducted to determine that free and non-free radicals play an important role in the elimination of
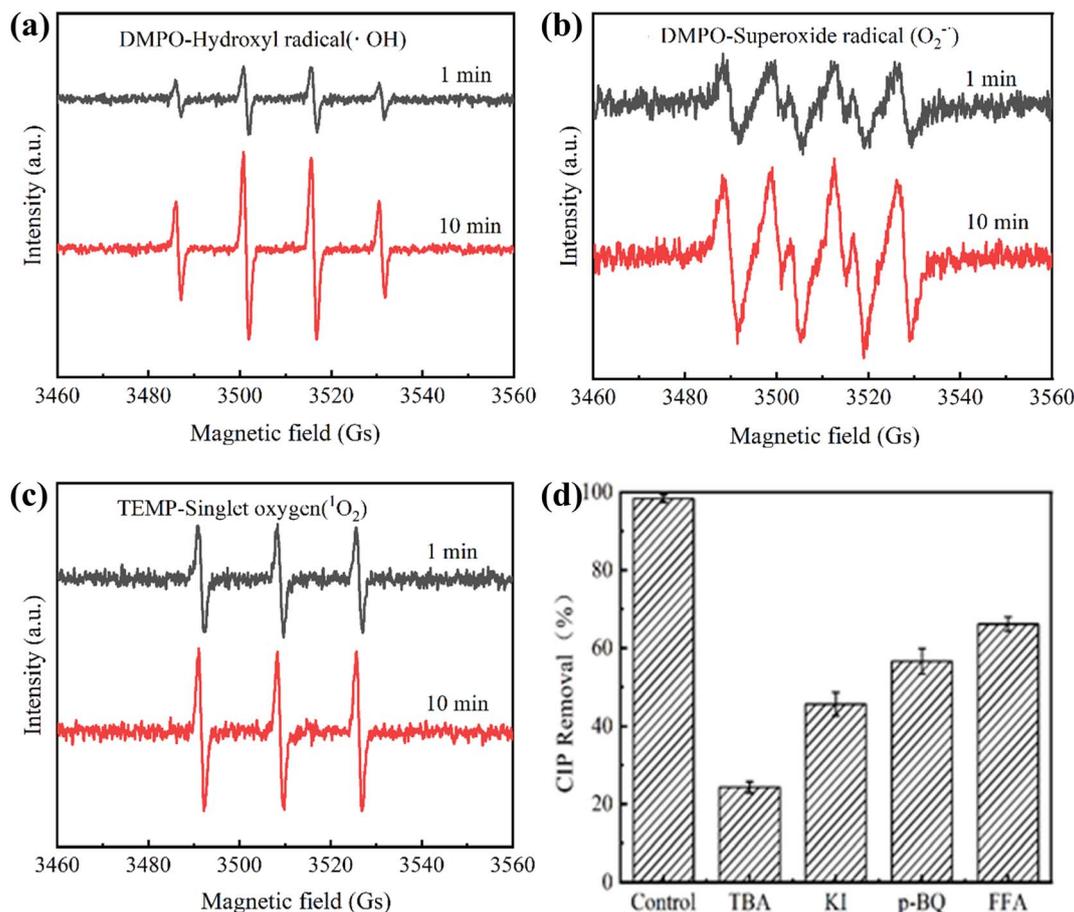
**Fig. 7** (a) EPR spectra at 1 min and 10 min in Fe–N-BC/$H_2O_2$: hydroxyl radical ($\cdot$OH); (b) superoxide radical ($\cdot O_2^-$); (c) singlet oxygen ($^1O_2$); (d) effects of different trapping agents on CIP removal.

CIP by Fe–N-BC/$H_2O_2$. Therefore, quenching experiments were conducted in various quenching agents. *tert*-Butanol (TBA) had a quenching effect on $\cdot$OH ($k = 4.8$–$7.6 \times 10^8$ M$^{-1}$ s$^{-1}$).[20] Potassium iodide (KI) was used to quench surface hydroxyl radical ($\cdot$OH$_{surf}$). *p*-benzoquinone (p-BQ) had a significant quenching effect on superoxide radical ($\cdot O_2^-$) ($k = 0.9$–$1.0 \times 10^9$ M$^{-1}$ s$^{-1}$).[20] Furfuryl alcohol (FFA) was a specific quencher for singlet oxygen ($^1O_2$) to confirm the existence of $^1O_2$.

According to Fig. 7(d), the removal effectiveness of CIP dramatically decreased when excessive amounts of tert-butanol (TBA), potassium iodide (KI), *p*-benzoquinone (p-BQ), and furfuryl alcohol (FFA) were added, respectively. The removal efficiency of CIP decreased from 98.25% to 24.31%, 45.68%, 56.62% and 66.19%, respectively. It showed that quenching test results were consistent with EPR test results in Fe–N-BC/$H_2O_2$ condition, which proved once again that the removal of CIP was accomplished by the oxidation of free radicals and non-free radicals.

In addition, it found that when excessive *tert*-butyl alcohol (TBA) was added, the inhibition of CIP degradation was stronger than other quencher agents. It showed that a large number of hydroxyl radicals and a small amount of superoxide free radicals and singlet oxygen were generated in the catalytic

reaction process. And the catalytic reaction mechanism was dominated by the surface hydroxyl radicals ($\cdot$OH$_{surf}$).

**3.3.2. The possible removal mechanism.** According to the EPR analysis and quenching test, the possible reaction mechanism of the degradation of ciprofloxacin under Fe–N-BC/$H_2O_2$ condition was explored (Fig. 8). The degradation of ciprofloxacin mainly occurred through two kinds of effects (*i.e.*, free radical and non-free radical). Hydrogen peroxide can be activated by iron doping on the surface of charcoal to form a hydroxyl radical. Nitrogen doping on the surface of biochar can induce the generation of free radicals and non-free radicals, and graphite nitrogen doping has good electron transfer performance.[33,47]

CIP was degraded by hydroxyl radicals ($\cdot$OH) (eqn (1)) and superoxide radicals ($\cdot O_2^-$), which were produced from the process of hydrogen peroxide and $O_2$ activated by the transition metal (Fe) (eqn (2)). Biochar can act as an electron donor, providing electrons directly to facilitate Fe(III) reduction, while persistent free radicals (PFRs) are generated during biochar pyrolysis.[20] Abundant PFRs had excellent catalytic degradation of refractory pollutants. Similar to transition metal activation of hydrogen peroxide, hydrogen peroxide can also be activated by PFRs to produce hydroxyl radicals ($\cdot$OH) (eqn (3)) to achieve
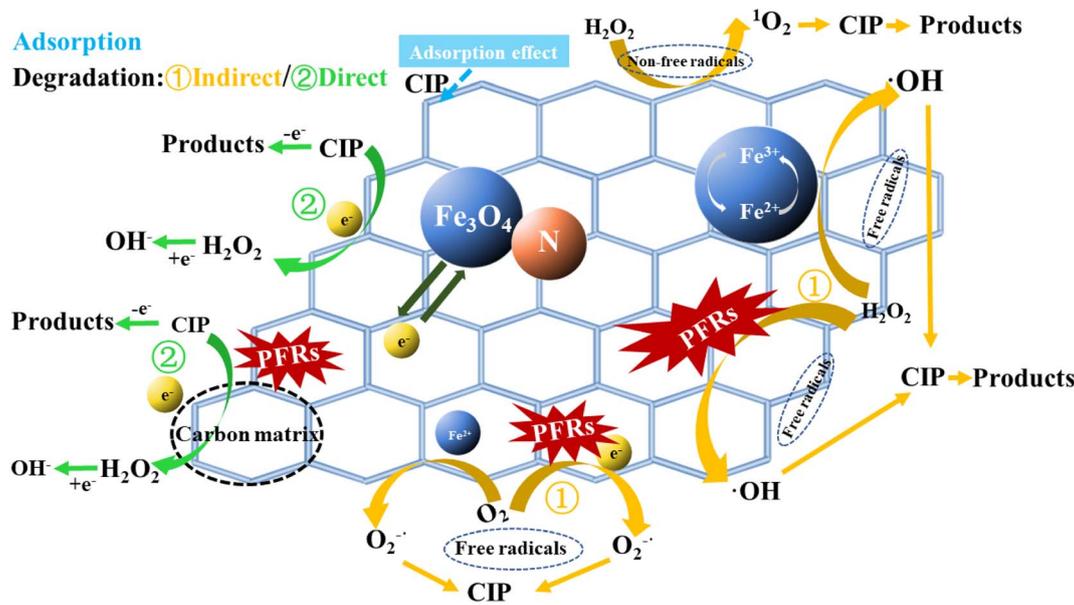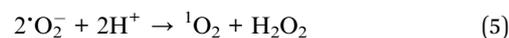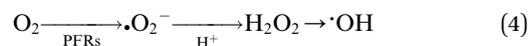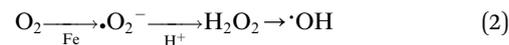
**Fig. 8** Mechanisms of CIP removal under Fe–N-BC/$H_2O_2$ condition.

effective removal of CIP. PFRs in biochar produce superoxide radicals ($\cdot O_2^-$) by both transferring electrons to oxygen molecules and directly activating hydrogen peroxide to produce reactive oxygen species (ROS) (eqn (4)). In addition, it was achieved through the recombination of superoxide radical ($\cdot O_2^-$) or the reaction of superoxide radical ($\cdot O_2^-$) with hydroxyl radical ($\cdot OH$) to generate singlet oxygen ($^1O_2$) (eqn (5)). Thus, the removal of CIP was achieved partly due to non-free radicals. Meanwhile, the O–O bond of hydrogen peroxide can be cleaved into hydroxyl radicals ($\cdot OH$), superoxide radicals ($\cdot O_2^-$) and singlet oxygen ($^1O_2$).

Persistent free radicals (PFRs) and iron in Fe–N-BC played a synergistic role in activating hydrogen peroxide and oxygen molecules to produce ROS. At the same time, persistent free radicals (PFRs) can directly degrade pollutants, although its oxidability was much lower than ROS. CIP can also be degraded directly by electron transfer due to the polyvalent state of iron. Therefore, both direct and indirect degradation were important ways pollutants removal by Fe–N-BC. In the conventional Fenton process, $\cdot OH$ produced by the reaction of $Fe^{2+}$ and $H_2O_2$ under acidic conditions is used for oxidative degradation of organic matter. Compared with the conventional Fenton process, the high specific surface area of Fe–N-BC endowed the system with strong adsorption capacity in this study. Meanwhile, the biochar acts as an electron donor, directly providing electrons to promote the reduction of Fe(III), while persistent free radicals (PFR) are generated during the pyrolysis of biochar. The electrons supplied by biochar react with $O_2$ to form $\cdot O_2^-$ and further to produce $^1O_2$. Therefore, in addition to the important role of $\cdot OH$ in the degradation of CIP, the $\cdot O_2^-$, $^1O_2$ and PFRs generated in the system also play a role. Additionally, the degradation of CIP by Fe–N-BC itself can be achieved through two pathways: (1) due to the larger specific surface area of Fe–N-BC, it can provide more surface-active sites, which can

have a higher adsorption rate for CIP.[48] (2) $O_2$ adsorbed on the catalyst surface as well as PFRs generated by BC during pyrolysis react with Fe to form $\cdot O_2^-$ (eqn (2) and (4)), which generates $^1O_2$ as well as $H_2O_2$ under acidic conditions for CIP oxidation (eqn (5)).[49]

$$Fe^{2+} + H_2O_2 \rightarrow Fe^{3+} + \cdot OH + OH^- \qquad (1)$$

$$O_2 \xrightarrow[\text{Fe}]{} \cdot O_2^- \xrightarrow[\text{H}^+]{} H_2O_2 \rightarrow \cdot OH \qquad (2)$$

$$BC + H_2O_2 \rightarrow BC^+ + \cdot OH + OH^- \qquad (3)$$

$$O_2 \xrightarrow[\text{PFRs}]{} \cdot O_2^- \xrightarrow[\text{H}^+]{} H_2O_2 \rightarrow \cdot OH \qquad (4)$$

$$2\cdot O_2^- + 2H^+ \rightarrow {}^1O_2 + H_2O_2 \qquad (5)$$

### 3.4. Possible degradation pathway

**3.4.1. Degradation pathways of CIP within the Fe–N-BC/$H_2O_2$ system.** By using HPLC-MS, the intermediate products CIP under Fe–N-BC/$H_2O_2$ condition were determined, and the possible degradation pathway was analyzed. The mass spectrum of intermediate products of CIP at different time is shown in Fig. S1.† The possible structure information of the intermediate products of CIP is listed in Table 1. As shown in Fig. 9, three possible degradation pathways during the degradation process were proposed.

In pathway I, piperazine rings in ciprofloxacin molecules were vulnerable to reactive oxygen species (hydroxyl radicals, superoxide radicals, etc.). The piperazine ring was oxidized by reactive oxygen to form a ring with a hydroxyl group. And then hydroxyl group was oxidized to a ketone group and opened to form product P1 ($m/z = 362$). The product P1 continued to be
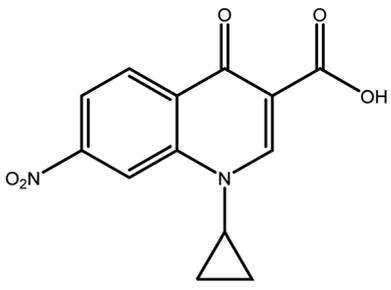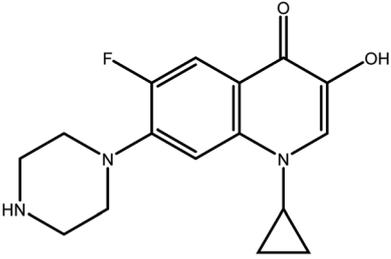
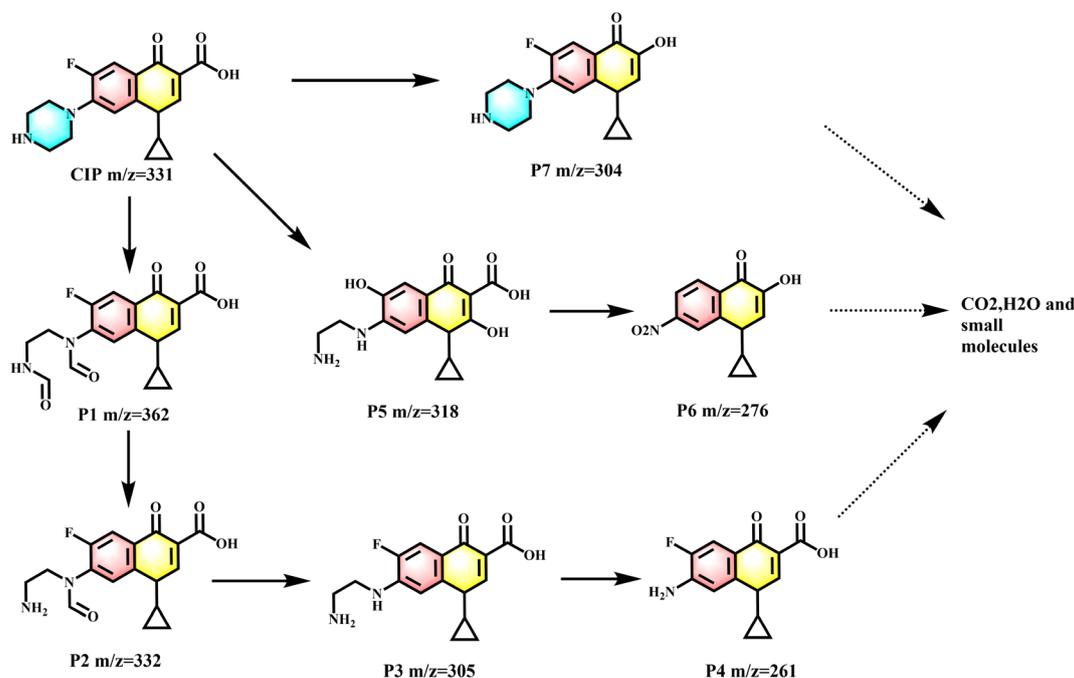**Table 1** Possible intermediates of CIP by catalytic hydrogen peroxide decomposition

| Compound | Formula | m/z | Structural formula |
|---|---|---|---|
| CIP | $C_{17}H_{18}FN_3O_3$ | 331 | |
| P1 | $C_{17}H_{16}FN_3O_5$ | 362 | |
| P2 | $C_{16}H_{16}FN_3O_4$ | 332 | |
| P3 | $C_{15}H_{16}FN_3O_3$ | 305 | |
| P4 | $C_{13}H_{11}FN_2O_3$ | 261 | |
| P5 | $C_{15}H_{17}N_3O_5$ | 318 | |

Table 1  (Contd.)

| Compound | Formula | $m/z$ | Structural formula |
| --- | --- | --- | --- |
| P6 | $C_{13}H_{10}N_2O_5$ | 276 | |
| P7 | $C_{16}H_{18}FN_3O_2$ | 304 | |



Fig. 9  Degradation pathways of the CIP in the Fe–N-BC/$H_2O_2$ system.

oxidized, losing a C=O bond successively, and successively transformed into the product P2 ($m/z = 332$) and P3 ($m/z = 305$). The piperazine ring was further oxidized by reactive oxygen species until it was completely removed to produce product P4 ($m/z = 261$). Finally, the product P4 was generated into small molecules such as $CO_2$ and $H_2O$ under continuous strong oxidation. Zhang *et al.* studied the degradation of CIP by Ce-OMS-2, which was similar to the pathway I of ciprofloxacin in this study.[50]

In pathway II, the oxidation of the piperazine ring by reactive oxygen species led to the breakage of the N–H bond on the ring, resulting in the production of the product P5 ($m/z = 318$). The product P5 was then further transformed to produce the P6 ($m/z = 276$). Eventually, small molecules such as $CO_2$ and $H_2O$ were formed.

In pathway III: carboxyl group on the quinolone ring of ciprofloxacin molecule was replaced by hydroxyl group to produce the product P7 ($m/z = 304$). The intermediate P7 was
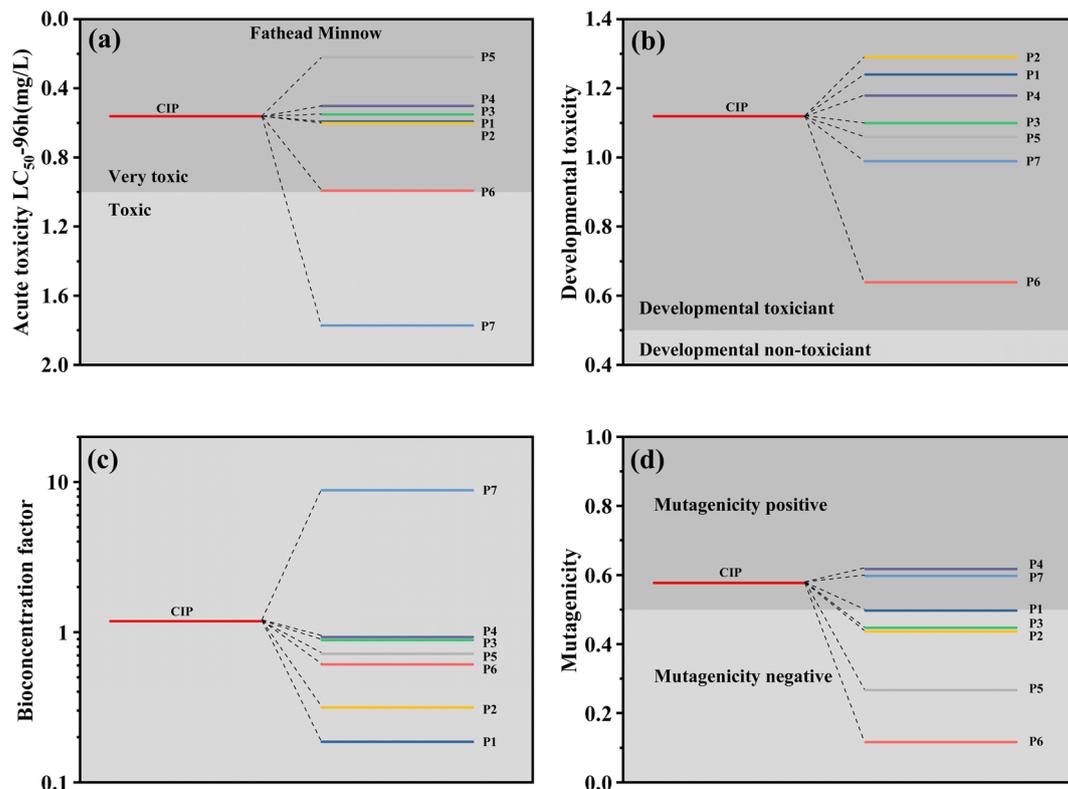
Fig. 10 (a) Fathead minnow $LC_{50}$ (96 h), (b) developmental toxicity, (c) bioaccumulation factor and (d) mutagenicity of CIP and its degradation products.

quickly oxidized by reactive oxygen species (ROS), yielding tiny molecules including $CO_2$ and $H_2O$.

**3.4.2. Degradation pathways of CIP within the general Fenton oxidation process.** The degradation pathway of CIP in the homogeneous Fenton process was summarized in Fig. S2.† In the conventional Fenton oxidation process, the ˙OH produced by the system attacks the piperazine ring in the structure of ciprofloxacin, leading to the loss of ethylene, followed by the excretion of piperazine from the ethylenediamine molecule or the formation of amino groups after partial ring opening, which is similar to pathway I in this study.[51–54] Simultaneously, P3 and P4 produced in this system are common intermediates in the Fenton oxidation CIP process. The difference is that in addition to pathway I in this study, we hypothesized two other pathways for CIP degradation by the intermediates detected by HPLC-MS. Based on EPR and reactive species capture experiments we know that reactive species (˙$O_2^-$, $^1O_2$) other than ˙OH are present within the Fe–N-BC/$H_2O_2$ system. Therefore, we extrapolated that the P4, P6 and P7 produced in the system, which are different from the conventional Fenton oxidation products, are due to the attack of other active substances on the CIP molecules.

**3.5. Toxicity assessment**

The toxicological properties of CIP and its degradation intermediates were examined by the toxicity estimates software program (T.E.S.T.) in order to further investigate the benefits of the oxidation process. Fathead minnow $LC_{50}$ (96 h),

developmental toxicity, bioaccumulation factor and mutagenicity are the main indexes. The $LC_{50}$ for fathead minnow and the developmental toxicity of CIP, respectively, were 0.56 mg $L^{-1}$ and 1.12, as shown in Fig. 10(a) and (b), and these values were categorized as "very toxic" and "developmental toxicant," respectively. Furthermore, the $LC_{50}$ values for most of CIP degradation products were higher than CIP. Notably, the $LC_{50}$ values of ultimate degradation P6 and P7 increased dramatically, indicating the production of low-toxicity compounds. In Fig. 10(c), the bioconcentration factor of all the products except P7 can decrease in the Fe–N-BC/$H_2O_2$ system. Fig. 10(d) further demonstrates that the degradation process may reduce mutagenicity slightly and that some degradation products are considered "mutagenicity negative". Additionally, the removal efficiency of TOC was 54.6%, futher revealing that the toxicity of CIP solution is considerably decreased.

## 4. Conclusion

Iron–nitrogen co-doped modified corncob (Fe–N-BC) was prepared by pyrolysis method in this study. The catalyst had a good removal performance, including abundant activation sites, good magnetic properties and a stable structure. When the concentration of $H_2O_2$ was 12 mM, pH was 4 and the dosage of Fe–N-BC was 0.6 g $L^{-1}$, CIP was virtually totally eliminated in 240 min. In a wide pH range, Fe–N-BC was found to have excellent efficiency, high stability, and good reusability. It was conducive to practical application. In Fe–N-BC/$H_2O_2$ condition,

EPR analysis and quenching experiments showed that the main mechanism of removal CIP was that the transition metal iron and persistent free radicals (PFRs) on the catalyst surface activated $H_2O_2$ to produce reactive oxygen species (ROS), including $^{\cdot}OH$, $^{\cdot}O_2^{-}$, $^1O_2$. The synergistic effect of transition metal and PFRs promoted the degradation of CIP. Meanwhile, pollutants can also be directly degraded by PFRs and electron transfer. Therefore, both direct and indirect action can degrade CIP. By using HPLC-MS analysis, seven potential intermediates for the breakdown of CIP were discovered and three possible degradation pathways were speculated: piperazine ring cleavage, defluorination and pyridine ring rupture. The toxicity and mutagenicity of pollutants has been reduced through the degradation process. This study provided new ideas and methods for the utilization of waste materials, the synthesis and implementation of innovative catalysts, and the remediation of organic contaminants.

## Conflicts of interest

The authors declare that they have no known competing financial interests or personal relationships that could have appeared to influence the work reported in this paper.

## References

1  X. Fan, Q. Lin, K. Xu, J. Zheng, J. Sun, H. Fu, Y. Liu, Y. Ma and J. He, *Sep. Purif. Technol.*, 2023, **316**, 123783.

2  Z. Zeng, Z. Deng, T. Wang, H. Huang and Y. Guo, *Sep. Purif. Technol.*, 2023, **311**, 123264.

3  Y. Zhang, J. Guo, B. Li, Z. Wang and Z. Xu, *J. Water Process. Eng.*, 2023, **56**, 104257.

4  Y. Li, L. Chen, X. Tian, L. Lin, R. Ding, W. Yan and F. Zhao, *Sci. Total Environ.*, 2021, **784**, 147049.

5  K. Sathishkumar, S. Naraginti, K. Lavanya, F. Zhang, R. Ayyamperumal and X. Liu, *Environ. Res.*, 2023, **235**, 116558.

6  X. Nie, G. Li, S. Li, Y. Luo, W. Luo, Q. Wan and T. An, *Appl. Catal. B*, 2022, **300**, 120734.

7  Z. Fang, Z. Lin, P. Chen, M. Feng, H. Liu, Z. Xiao, Z. Lin, D. Li, D. Liu, Y. Zhang, W. Lv and G. Liu, *J. Clean. Prod.*, 2023, **414**, 137706.

8  J. Zhu, H. Wang, A. Duan and Y. Wang, *J. Hazard. Mater.*, 2023, **446**, 130676.

9  W. Xu, X. Zheng, Z. Shangguan, J. Qu and W. Zhang, *Chem. Eng. J.*, 2023, **464**, 142562.

10  V. Subhiksha, M. K. Okla, P. R. Sivaranjani, M. A. Abdel-Maksoud, I. A. Saleh, H. A. Abu-Harirah and S. S. Khan, *Chemosphere*, 2023, **342**, 140181.

11  E. Yakamercan, A. Aygün and H. Simsek, *J. Environ. Sci.*, 2023, DOI: 10.1016/j.jes.2023.08.013.

12  L. Qin, W. Chen, Y. Fu, J. Tang, H. Yi, L. Li, F. Xu, M. Zhang, W. Cao, D. Huang and C. Lai, *Chem. Eng. J.*, 2022, **449**, 137840.

13  K. Chen, T. Li, X. Zhang, B. Lei, Z. Li and Y. Xu, *J. Environ. Chem. Eng.*, 2023, **11**, 110651.

14  S. Karoui, W. A. Saoud, A. Ghorbal, F. Fourcade, A. Amrane and A. A. Assadi, *J. Water Process. Eng.*, 2022, **50**, 103207.

15  D. Zheng, J. Zou, H. Xu, M. Wu, Y. Wang, C. Feng, E. Zheng, T. Wang, Y. Shi, Y. Chen and B. Li, *Chemosphere*, 2023, **325**, 138387.

16  J. Zhang, M. Liu, B. Pang, C. Liu, J. Ma, J. Niu and R. Zhang, *Sep. Purif. Technol.*, 2023, **325**, 124676.

17  Q. Jin, W. Liu, Y. Dong, Y. Lu, C. Yang and H. Lin, *J. Clean. Prod.*, 2023, **423**, 138688.

18  L. Lin, J. Wang, Z. Zhao, J. Zhu, A. Zhamaerding, L. Feng, D. Yang, L. Meng, C. He, W. Wang, Y. Zhang and W. Jin, *Chem. Eng. J.*, 2023, **474**, 145600.

19  C. Dong, W. Fang, Q. Yi and J. Zhang, *Chemosphere*, 2022, **308**, 136205.

20  F. Deng, Q. Chen, Y. Zhu, X. Liang, R. Zhu and Y. Xi, *Chem. Eng. J.*, 2023, **473**, 144946.

21  Y. Pan, Y. Zhang, M. Hou, J. Xue, R. Qin, M. Zhou and Y. Zhang, *Sep. Purif. Technol.*, 2023, **317**, 123905.

22  Y. Lu, X. Qin, K. Wang, S. Chen and X. Quan, *Sep. Purif. Technol.*, 2023, **320**, 124196.

23  H. Zhu, Q. An, A. Syafika Mohd Nasir, A. Babin, S. Lucero Saucedo, A. Vallenas, L. Li, S. A. Baldwin, A. Lau and X. Bi, *Bioresour. Technol.*, 2023, **388**, 129745.

24  Y. Zhou, S. Y. Leong and Q. Li, *J. Water Process. Eng.*, 2023, **55**, 104222.

25  S. Zeng and E. Kan, *Chemosphere*, 2022, **306**, 135554.

26  L. Liu, R. Yu, S. Zhao, X. Cao, X. Zhang and S. Bai, *J. Environ. Manage.*, 2023, **335**, 117576.

27  P. Kumar, A. K. Patel, R. R. Singhania, C.-W. Chen, R. G. Saratale and C.-D. Dong, *Bioresour. Technol.*, 2023, **388**, 129654.

28  X. Zhao, X. Li, Y. Xu, Y. Qi, Q. Wei and X. Jia, *J. Water Process. Eng.*, 2023, **52**, 103569.

29  S. Ahmad, L. Liu, S. Zhang and J. Tang, *J. Hazard. Mater.*, 2023, **446**, 130727.

30  S. Ma, D. Chen, Y. Zhong, Y. Feng, Z. He, W. Zhang, Y. Zhang, H. Ding and X. Wu, *Chem. Eng. J.*, 2023, **467**, 143385.

31  N. Zhang, B. Zhang, A. He, H. Sun, C. Wang, Z. Wen, G. Yan, Y. Ma and R. Xue, *J. Environ. Chem. Eng.*, 2023, **11**, 110717.

32  Y. Li, H. Ding, L. Qu, L. Bian, G. Ren and Q. Hu, *Adv. Powder Technol.*, 2023, **34**, 104186.

33  X. Li, J. Xu and Z. Yang, *Chem. Eng. J.*, 2022, **450**, 138466.

34  Z. Jiang, J. Wei, Y. Zhang, X. Niu, J. Li, Y. Li, G. Pan, M. Xu, X. Cui, N. Cui and J. Li, *J. Cleaner Prod.*, 2023, **384**, 135641.

35  J. Wang, X. Cheng, P. Li, Q. Fan, D. Wu and H. Liang, *Chemosphere*, 2023, **341**, 140044.

36  Z. Liu, R. Chen, M. Li, S. Yang, J. Zhang, S. Yuan, Y. Hou, C. Li and Y. Chen, *J. Hazard. Mater.*, 2023, **459**, 132089.

37  J. Liu, Y. Zhang, Y. Dong, Z. Jiang, L. Zhang, W. Liu, J. Guan and H. Lin, *Sep. Purif. Technol.*, 2024, **328**, 125034.

38  H. Zhang, Y. Yu, Y. Li, L. Lin, C. Zhang, W. Zhang, L. Wang and L. Niu, *Chemosphere*, 2023, **317**, 137888.

39  K. Zhang, D. Huang, Y. Zhang, N. El Houda Bouroubi, P. Chen, N. Ganbold, P. He, J. Liu, Y. Fang, M. Gan, J. Zhu and B. Yang, *J. Environ. Manage.*, 2023, **335**, 117540.

40 J. Lei, Y. Han, C. Zhao, S. Zhang, F. Han, Z. Li, J. Hao and W. Zhou, *Sep. Purif. Technol.*, 2023, **324**, 124591.

41 H. Tian, K. Cui, S. Sun, J. Liu and M. Cui, *Sep. Purif. Technol.*, 2023, **322**, 124249.

42 J. Huang, M. Wang, S. Luo, Z. Li and Y. Ge, *Environ. Res.*, 2023, **219**, 115166.

43 Z. Ren, Z. Wang, L. Lv, P. Ma, G. Zhang, Y. Li, Y. Qin, P. Wang, X. Liu and W. Gao, *J. Environ. Manage.*, 2022, **316**, 115213.

44 W. Xia, S. Li, G. Wu and J. Ma, *J. Hazard. Mater.*, 2023, **460**, 132377.

45 D. Liu, A. Guo, Y. Qi, Z. Ji, H. Li, X. Cao, Z. Zhang, X. Zhang, K. Wu and A. Cai, *Sep. Purif. Technol.*, 2023, **329**, 125322.

46 L. Li, M. Cheng, L. Qin, E. Almatrafi, X. Yang, L. Yang, C. Tang, S. Liu, H. Yi, M. Zhang, Y. Fu, X. Zhou, F. Xu, G. Zeng and C. Lai, *Sci. Total Environ.*, 2022, **828**, 154188.

47 P. Huang, P. Zhang, C. Wang, J. Tang and H. Sun, *Appl. Catal. B*, 2022, **303**, 120926.

48 Y. Zhao, X. Yuan, X. Li, L. Jiang and H. Wang, *J. Hazard. Mater.*, 2021, **409**, 124893.

49 B. Zhang, X. Shan, J. Yu, H. Zhang, K. Tawfik Alali, Q. Liu, J. Zhu, J. Yu, J. Liu, R. Li and J. Wang, *Sep. Purif. Technol.*, 2024, **328**, 125026.

50 L. Zhang, J. Tu, L. Lyu and C. Hu, *Appl. Catal. B*, 2016, **181**, 561–569.

51 A. S. Giri and A. K. Golder, *RSC Adv.*, 2014, **4**, 6738–6745.

52 A. Gupta and A. Garg, *Chemosphere*, 2018, **193**, 1181–1188.

53 S. K. Mondal, A. K. Saha and A. Sinha, *J. Clean. Prod.*, 2018, **171**, 1203–1214.

54 E. S. Elmolla and M. Chaudhuri, *J. Hazard. Mater.*, 2009, **172**, 1476–1481.